Trajectory Generation via FIR Filters: a Procedure for Time-Optimization under Kinematic and Frequency Constraints

Luigi Biagiotti[a,*], Claudio Melchiorri[b]

[a] *Department of Engineering "Enzo Ferrari", University of Modena and Reggio Emilia, Strada Vignolese 905, 41100 Modena, Italy*
[b] *Department of Electrical, Electronic and Information Engineering "Guglielmo Marconi", University of Bologna, Viale Risorgimento 2, 40136 Bologna, Italy*

Abstract

This paper starts from the results reported in the article "FIR Filters for Online Trajectory Planning with Time- and Frequency-Domain Specifications", where the use of a cascade of FIR (Finite Impulse Response) filters for planning minimum-time multi-segment polynomial trajectories, i.e. trajectories composed of several polynomial segments, under constraints of velocity, acceleration, etc. is proposed. In particular, in that paper the relationship between the limits acting on the trajectory derivatives (i.e. velocity, acceleration, jerk, etc.), and the parameters of the filters is deduced, along with a set of constraints among these parameters that guarantees the time-optimality of the trajectory in the rest-to-rest case, that is with null boundary conditions on the trajectory derivatives. However, the choice of the parameters, when these conditions are not satisfied, was still an open problem, at least

* *Corresponding author.* Tel.:+390592056315; fax:+390592056329.
Email addresses: luigi.biagiotti@unimore.it (Luigi Biagiotti), claudio.melchiorri@unibo.it (Claudio Melchiorri)

for high order trajectories. In this paper, we show that in case the conditions are not met by the filters parameters, the optimality of the trajectory under the given kinematic bounds can be assured in any case. An algorithm for the selection of the optimal parameters for a generic n-th order trajectory planner subject to n kinematic limits is provided. Additionally, the optimal combination of kinematic and frequency constraints is considered. In fact, the compliance with these two types of constraints may lead to a planner composed by a redundant number of filters and, therefore, a procedure for the selection of the minimum number of FIR filters is devised. The effectiveness of the time-optimal trajectory planner is proved by means of numerical simulations and experimental tests.
Keywords: Trajectory planning, Multi-segment trajectories, Smoothers, Shaping filters, Minimum-time trajectories, Residual vibrations suppression

1. Introduction

Motion control systems used in industry are required to be more and more responsive when unforseen events occur or manufacturing demands change. For this reason, there is a growing need for trajectory planning algorithms that provide, possibly online, smooth motion profiles. The reference trajectories must guarantee high tracking accuracy and avoid exciting natural vibration modes of the mechanical structure. Moreover, they must be compliant with the kinematic limits, i.e. torque, acceleration and jerk, imposed by the actuators. The minimum-duration is another basic requirement. In the industrial practice and in the scientific literature, several solutions have been proposed but each of them shows pros and cons. They are typically based

on a combination of polynomial profiles, such as trapezoidal velocity, acceleration, and jerk profiles, see Erkorkmaz and Altintas (2001); Lambrechts et al. (2005); Biagiotti and Melchiorri (2008) among many others. The most straightforward technique consists in the formulation of the trajectory via its analytical expression, but unfortunately its complexity grows exponentially as the required order n, i.e. the number of bounded derivatives and accordingly the number of desired kinematic constraints, increases. As a matter of fact, these types of trajectories are a combination of a number of properly joined segments, that may range from one up to $2^n - 1$, according to the constraints and the boundary conditions. Therefore, the analytical expression of the trajectory, that should take into account all the possible cases, is combined with a decision tree that determines the specific structure that the motion profile must have on the basis of the given inputs (constraints and boundary conditions). This approach has been successfully used to design online optimal trajectory planners with $n = 2$ [Kroger et al. (2006)] and $n = 3$ [Kroger and Wahl (2010)], but the high complexity of this method does not allow to plan higher order trajectories.

Alternative solutions are based on properly tuned dynamic systems which filter and smoothen rough commands, like step signals, that specify the target position [see Zanasi et al. (2000); Zanasi and Morselli (2003); Zheng et al. (2009); Biagiotti and Zanasi (2010); Bianco and Ghilardelli (2014)]. These systems are generally designed as a chain of integrators with cascaded feedback control loops, that allow minimum-time tracking of the reference input with saturated control input and saturated internal state variables. However, also in this case the solutions proposed in the literature are limited to third

order trajectories.

In order to cope with this limitation, some simplificative assumptions have been introduced on the constraints, supposed e.g. symmetric, and on the boundary conditions, by assuming for instance that initial/final velocity/acceleration are null. In this way, in Lambrechts et al. (2005) a fourth order rest-to-rest symmetric trajectory is determined analytically, by computing the closed-form expression of the application time-instants and of the durations of the impulses composing the snap profile, which is integrated four times to obtain the position. It is worth mentioning that the proposed solution is optimal only if the maximum velocity is actually reached. Moreover this technique is specifically designed for trajectories with $n = 4$ and cannot be generalized to higher order motions.

General solutions in terms of trajectory order are proposed in Nguyen et al. (2008), Knierim and Sawodny (2012) and Ezair et al. (2014), where numerical procedures for the computation of the parameters of a generic n-th order trajectory are devised. Because of their algorithmic nature, the use of the two above mentioned methods may be critical in online applications, specially when n assumes large values. Moreover, they do not guarantee the optimality of the resulting trajectory. For instance the approach proposed by Ezair et al. (2014) is based on the hypothesis, not always valid, that all the given bounds are reached by the trajectory and its derivatives.

A very promising method for time-optimal trajectory generation is based on a cascade of FIR filters, and, in particular, of moving average filters. This type of filters has been used in several applications for smoothen a given reference signal, with the usual purpose of reducing vibrations in resonant

systems, see for instance Nozawa et al. (1985); Kim et al. (1994); Chen and Lee (1998); Jeon and Ha (2000). In fact, one of the main advantages that this approach offers with respect to the above mentioned methods for trajectory planning/smoothing is the possibility of shaping the frequency spectrum of the output trajectory. This feature of FIR filters has been mixed with the compliance to kinematic constraints, which is typical of trajectory generators. In Biagiotti and Melchiorri (2012) the proposed online trajectory generator is based solely on a cascade of FIR filters, while in Besset and Bearee (2017) a FIR filter is combined with the analytical expression of a second order trajectory with the aim of joining the efficiency and the low complexity of the filter with the flexibility given by the closed-form expression of the trajectory. In Sencer et al. (2015); Tajima et al. (2018), chains of FIR filters are used in interpolation problems for online planning of multi-dimensional trajectories with time and frequency specifications. In the field of multi-dimensional interpolation, it is worth mentioning that also B-splines can be generated via a chain of FIR filters, see Biagiotti and Melchiorri (2011, 2013).

Despite the wide literature on FIR filters based trajectory planners, some open problems still remains. In particular, the results presented so far do not guarantee the time-optimality of the trajectory for any set of kinematic constraints even in the rest-to-rest case. This problem is highlighted in Biagiotti and Melchiorri (2012), where it is shown that the expressions relating the kinematic bounds with the filters parameters (which is used by all the above cited works in order to take into account the kinematic constraints) is valid only under certain conditions. One of the main contributions of this paper consists in a procedure for the computation of the parameters that

provides the optimal solution, for rest-to-rest trajectories of any order, starting from any set of constraints.

Secondly, the optimal combination of kinematic and frequency conditions in the design of the trajectory generator has been tackled. As a matter of fact, by simply considering an additional FIR filter for any constraint, as proposed in the literature, the trajectory filter may be redundant, in the sense that some filters can be unnecessary. In this paper, a procedure for the computation of the minimum number of filters, that guarantees the compliance with all the specifications, and of their parameters is proposed. By means of some experimental tests on a resonant systems, i.e. a flexible link, the effectiveness and the advantages of the proposed technique are demonstrated. In particular, we have proved that an integrated solution to the problems of compliance with kinematic limits and of vibration suppression may lead to motion profiles shorter in time with respect to the application of a filtering action, like for instance a Zero Vibration (ZV) input shaper, to trajectories already compatible with the required bounds but guarantees similar levels of residual vibrations.

The above mentioned procedures for the optimization of the chain of filters, which have been implemented in the Matlab language, have been collected in Matlab/Simulink toolbox that computes the optimal filters parameters for a given set of constraints and then builds the Simulink block-scheme model of the trajectory generator (in Biagiotti (2019) the link to download this tool is reported).

The paper is organized as follows. In Sec. 2 the problem of trajectory generation by means of a particular type of FIR filters, called *rectangular smoothers*,

is briefly summarized. Then, in Sec. 3 the procedure for the computation of the optimal filters parameters under kinematic limits is presented, and its working mode is illustrated in Sec. 4 with some numerical examples. Then, the optimization of the trajectory generator with the addition of frequency constraints is presented in Sec. 5 and experimentally tested in Sec. 6. Concluding remarks are provided in the last section.

2. Multi-segment trajectories generation via rectangular smoothers

In Biagiotti and Melchiorri (2012), it is shown that a multi-segment trajectory $q_n(t)$ of order n, compliant with the symmetric constraints

$$q_{min}^{(i)} = -q_{max}^{(i)}, \quad i = 1, \ldots, n$$

can be obtained by filtering a step input with a cascade of n dynamic filters characterized by the transfer function

$$M_i(s) = \frac{1}{T_i} \frac{1 - e^{-sT_i}}{s} \tag{1}$$

where the parameter T_i (in general different for each filter composing the chain) is a time length, see Fig. 1. Note that the expression of filters, that in the field of the trajectory planning are called *rectangular smoothers*, coincides with the transfer function of a standard moving average filter.

The resulting trajectory $q_n(t)$ is composed by several polynomial segments defined as linear combination of the basis functions t^i, $i = 0, \ldots, n$. The smoothness of the trajectory, that is the number of continuous derivatives, is strictly tied to the number of filters composing the chain. If n filters are considered, the resulting trajectory will be of class $\mathcal{C}^{n-1}$. The generic

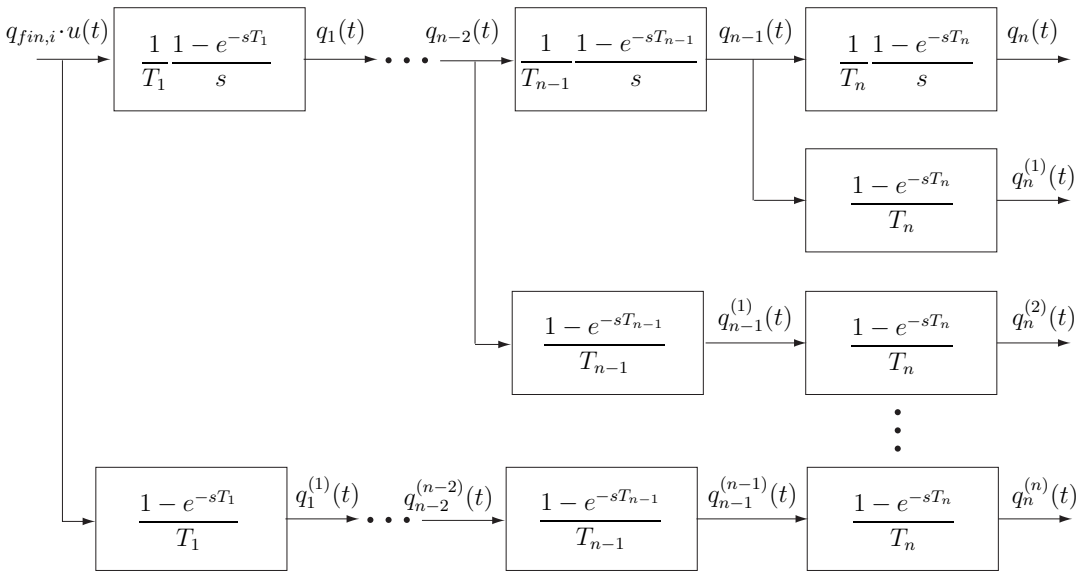

Figure 1: System composed by n filters for the computation of an optimal trajectory $q_n(t)$ of class $\mathcal{C}^{n-1}$ and of all the derivatives $q_n^{(i)}(t)$ of order $i = 1, \ldots, n$.

j-th derivative $q_n^{(j)}(t)$ is composed by polynomial functions which are linear combination of t^i, $i = 0, \ldots, n-j$ and the n-th derivative $q_n^{(n)}(t)$ is necessarily formed by constant segments. Note that, as shown in Fig. 1, the proposed trajectory generator provides all the derivatives up to the order n together with the trajectory $q_n(t)$.

By increasing the smoothness of the trajectory, adding filters in the chain, its duration augments as well. As a matter of fact, the total duration of a trajectory planned by means of n dynamic systems $M_i(s)$ is simply given by the sum of the lengths of the impulse response of each filter, i.e.

$$T_{tot} = T_1 + T_2 + \ldots + T_n.$$

The parameters T_i are generally set with the purpose of imposing desired bounds on velocity, acceleration, jerk and higher derivatives, by simply assuming

$$\begin{aligned} T_1 &= \frac{h}{q_{max}^{(1)}} \\ T_i &= \frac{q_{max}^{(i-1)}}{q_{max}^{(i)}}, \quad i = 2, \ldots, n \end{aligned} \tag{2}$$

where h denotes the maximum required displacement, i.e. $h = \max_i |q_{fin,i} - q_{in,i}|$ being $q_{in,i}$ and $q_{fin,i}$ the starting and the ending position of the i-th trajectory segment composing the motion profiles.

However, conditions (2) alone do not assure the time-optimality of the trajectory and the compliance with all the limits $q_{max}^{(i)}$, $i = 1, \ldots, n$, but it is also necessary that the time-lengths T_i found with (2) meet the conditions

$$\begin{aligned} T_1 &\geq T_n + \ldots + T_2 \\ T_2 &\geq T_n + \ldots + T_3 \\ &\vdots \\ T_{n-2} &\geq T_n + T_{n-1} \\ T_{n-1} &\geq T_n \,, \end{aligned} \tag{3}$$

see Biagiotti and Melchiorri (2012) for more details. The fact that inequalities (3) are not satisfied does not mean that a time-optimal multi-segment trajectory compliant with all the constraints cannot be generated by the filters chain but that the parameters found with (2) do not lead to such a trajectory and, therefore, it is necessary to modify their values. In the next section a procedure for the computation of the optimal parameters T_i with any set of limits is proposed.

3. Parameters modification for the time-optimality of the trajectory

Given a trajectory generator composed by n filters, the verification of conditions (3) proceeds from the last relation, involving only T_{n-1} and T_n, towards the first one, in which all the constants T_i appear. Let us consider a generic condition that can be rewritten in a compact form as

$$T_i \geq \sum_{k=i+1}^{n} T_k, \qquad i = 1, \ldots, n-1. \tag{4}$$

Since the parameters T_i are computed according to (2), the condition (4) can be written as

$$\frac{q_{max}^{(i-1)}}{q_{max}^{(i)}} \geq \frac{q_{max}^{(i)}}{q_{max}^{(i+1)}} + \sum_{k=i+2}^{n} T_k, \qquad i = 1, \ldots, n-1. \tag{5}$$

where the term $\sum_{k=i+2}^{n} T_k$ does not depend on $q_{max}^{(i)}$. As a consequence, if for the i-th parameter T_i the inequality is not verified, it is possible to act by decreasing the value of $q_{max}^{(i)}$ in order to make (5) true. Note that the reduction of $q_{max}^{(i)}$ has a twofold effect: on the one hand it increases the value of $T_i = \frac{q_{max}^{(i-1)}}{q_{max}^{(i)}}$ on the left side, on the other hand it reduces $T_{i+1} = \frac{q_{max}^{(i)}}{q_{max}^{(i+1)}}$ in the right side. Specifically, the new limit value $\hat{q}_{max}^{(i)} = \alpha q_{max}^{(i)}$ is assumed, where α is a positive constant strictly smaller than 1. The new values of T_i and T_{i+1} are

$$\hat{T}_i = \frac{T_i}{\alpha}, \quad \hat{T}_{i+1} = \alpha T_{i+1} \tag{6}$$

and, accordingly, equation (5) becomes

$$\frac{T_i}{\alpha} \geq \alpha\, T_{i+1} + \sum_{k=i+2}^{n} T_k, \qquad i = 1, \ldots, n-1. \tag{7}$$

By iteratively applying (6) it is possible to met the condition (7). However, the modification of the parameter T_{i+1}, that allows to comply with (7) for a generic index i, may cause to violate the condition for $i+1$. For this reason, at each modification it is necessary to check if the previous condition still holds true and, if not, the procedure above outlined must be repeated. For the sake of clarity, a schematic representation of the algorithm for parameters selection and optimization is illustrated in Fig. 2. The constant value of α determines the velocity of convergency of the algorithm and the precision of the solution: values closer to 1 produce more accurate solutions but require a larger number of iterations and vice-versa. In order to improve the velocity of the algorithm by reducing the number of iterations without worsen the accuracy of the solution a varying value of α can be adopted. In particular, the limit value of α, i.e. the maximum value of α that makes (7) true can be found by solving the second-degree equation

$$T_{i+1}\,\alpha^2 + \left(\sum_{k=i+2}^{n} T_k\right)\alpha - T_i = 0. \tag{8}$$

The positive solution of (8) to be inserted in (6) is

$$\alpha = -\frac{\sum_{k=i+2}^{n} T_k}{2T_{i+1}} + \sqrt{\left(\frac{\sum_{k=i+2}^{n} T_k}{2T_{i+1}}\right)^2 + \frac{T_i}{T_{i+1}}}. \tag{9}$$

Unfortunately, by using (9) the vector of parameters T_k may converge to a suboptimal solution, i.e. not minimum-time, if the modification occurring on T_{i+1} and T_i is very large (that is α is rather small) and requires a variation on T_k, $k = i+2, \ldots, n$. A simple and effective way to avoid this drawback consists in limiting the minimum value of α to a value α_{min} close enough to one. The Matlab code of the recursive function implementing the procedure

based on the variable α is reported in Appendix A. Note that α is also bounded from above. The limit value α_{max} is imposed to prevent infinite recursions caused by the numerical rounding of α to one.

In order to estimate the computational efficiency of the proposed tech-

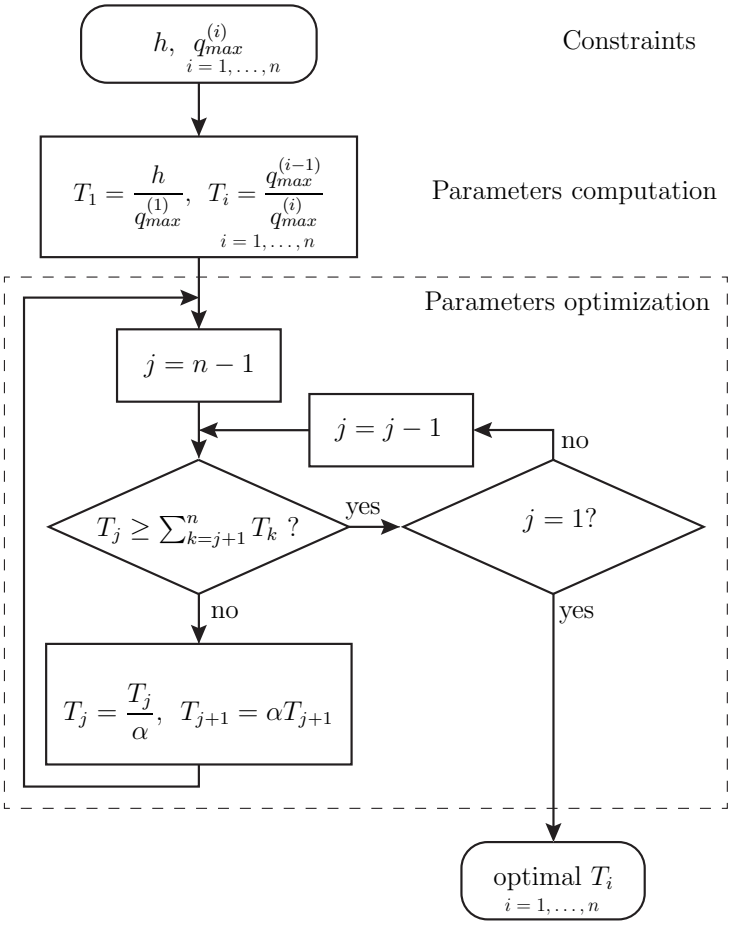

Figure 2: Flowchart for parameters selection and optimization of a n-th order trajectory generator.

Order n	2	3	4	5	6
# iterations (constant α)	3715	8151	15297	25538	34506
# iterations (variable α)	69	219	436	2712	12599

Table 1: Maximum number of iterations required by the optimization procedure in 10^6 tests based on vectors $\boldsymbol{T} = [T_i]$, $i = 1, \ldots, n$ chosen randomly in the interval $[0.01, 10]$ s.

niques a number (10^6) of random tests have been performed and the worst case scenario, i.e. with the maximum number of iterations, has been considered. Table 1 summarizes the results for different orders n both with constant parameter $\alpha = 0.999$ and with α variable in the range $[\alpha_{min}, \alpha_{max}] = [0.95, 0.999999]$. Even if the rate of growth in the latter case is higher than in the former, the number of required iterations is drastically reduced. The combination of the limited number of iterations and the simple calculations required by each of them makes the procedure suitable also for online trajectory planning.

4. Numerical examples of optimal multi-segment trajectories with kinematic constraints

In order to show the effectiveness of the proposed approach, a fourth order trajectory planner is considered, i.e. a system composed by 4 rectangular smoothers. A general closed-form solution of the motion trajectory produced by this type of planner, which is called *limited snap trajectory* or *fifteen-segment trajectory*, does not exist in the literature and the solutions proposed e.g. in Lambrechts et al. (2005) or in Ezair et al. (2014) are based on the assumption that the bounds on velocity and/or higher order deriva-

Trajectory No.	h	$q_{max}^{(1)}$	$q_{max}^{(2)}$	$q_{max}^{(3)}$	$q_{max}^{(4)}$
1	10	3	0.4	0.4	5
2	0.4	3	0.4	0.4	5
3	10	1.5	0.4	4	5
4	10	3	5	5	5

Table 2: Kinematic limits considered for the computation of the parameters of the filters composing a fourth order trajectory generator.

Trajectory No.	T_1	T_2	T_3	T_4	T_{tot}
1	3.3333	7.5	1	0.08	11.9133
2	0.1333	7.5	1	0.08	8.7133
3	6.6667	3.75	0.1	0.8	11.3167
4	3.3333	0.6	1	1	5.9333

Table 3: Parameters T_i of the forth order trajectory planner computed according to (2) on the basis of the kinematic constraints reported in Tab. 2.

tives are all reached. Note that this hypothesis is exactly equivalent to (3). In order to show how the proposed technique works, four different trajectory planning problems have been considered. The kinematic constraints imposed in each of them are reported in Tab. 2, while Tab. 3 contains the corresponding values of the parameters T_i, computed according to the standard relationships (2), and the total duration T_{tot} of the resulting trajectories. Finally, in Tab. 4 the new parameters T_i, obtained after the optimization procedure described in Sec. 3, and the consequent total duration of the trajectory are shown.

Trajectory No.	T_1	T_2	T_3	T_4	T_{tot}
1	5.5691	4.4891	1	0.08	11.1382
2	1.6426	0.8213	0.7413	0.08	3.2851
3	6.6667	3.75	0.2828	0.2828	10.9824
4	3.3333	1.3390	0.6694	0.6694	6.0111

Table 4: Parameters T_i obtained by applying the optimization procedure described in Sec. 3 to the initial parameters reported in Tab. 3.

The initial parameters that define the first trajectory, denoted as trajectory No. 1, do not satisfy condition (3) for $i = 1$. On the basis of (4), it is clear that it is necessary to act by progressively reducing the bound $q_{max}^{(1)}$ in order to achieve the time-optimality of the motion. As a matter of fact, the trajectory profiles in Fig. 3(a) shows that the motion is not minimum-time since there is a time interval (highlighted in all the figures with a grey background) in which none of the derivatives of the motion profile reaches the corresponding bound. In particular, in this interval the velocity ${q_4}^{(1)}(t)$ maintain a constant value which is strictly smaller than $q_{max}^{(1)}$, while all the other derivatives are zero. The application of the proposed optimization procedure on the parameters T_i leads to the motion profiles of Fig. 3(b), with a reduction of the total duration of the trajectory of -6.50%. In this case, even if the maximum velocity obtained is still strictly smaller than the given bound, a time interval where this value is kept constant no longer exists. Therefore, the initial trajectories characterized by $2^n - 1$ different tracts, that is a standard 15 segments trajectory considering $n = 4$, becomes a 14 segments trajectory. Moreover, in every time-instant a derivative of the planned tra-

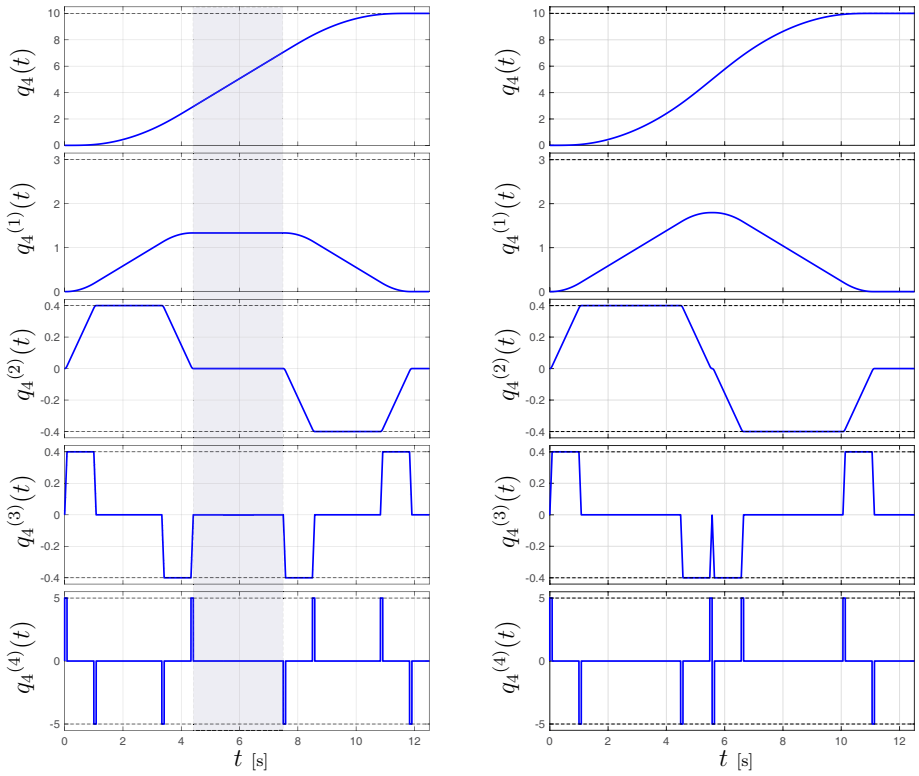

(a) (b)

Figure 3: Profiles of position, velocity, acceleration, jerk and snap of the trajectories No. 1 obtained with a cascade of four rectangular smoothers with the parameters reported in Tab. 3 (a) and in Tab. 4 (b).

jectory equals the corresponding bound. As a consequence, the trajectory, which is still compliant with the given kinematic constraints, cannot be further reduced in duration without violating one of these constraints and thus the new trajectory is optimal in time, at least by considering the typical pattern of multi-segment trajectories in which the velocity is composed by three phases (acceleration, constant velocity, deceleration), the acceleration/deceleration phases are in turn composed by three phases and so on, for a total of $2^n - 1$ different segments. As highlighted with a red circle in Fig. 4(a),

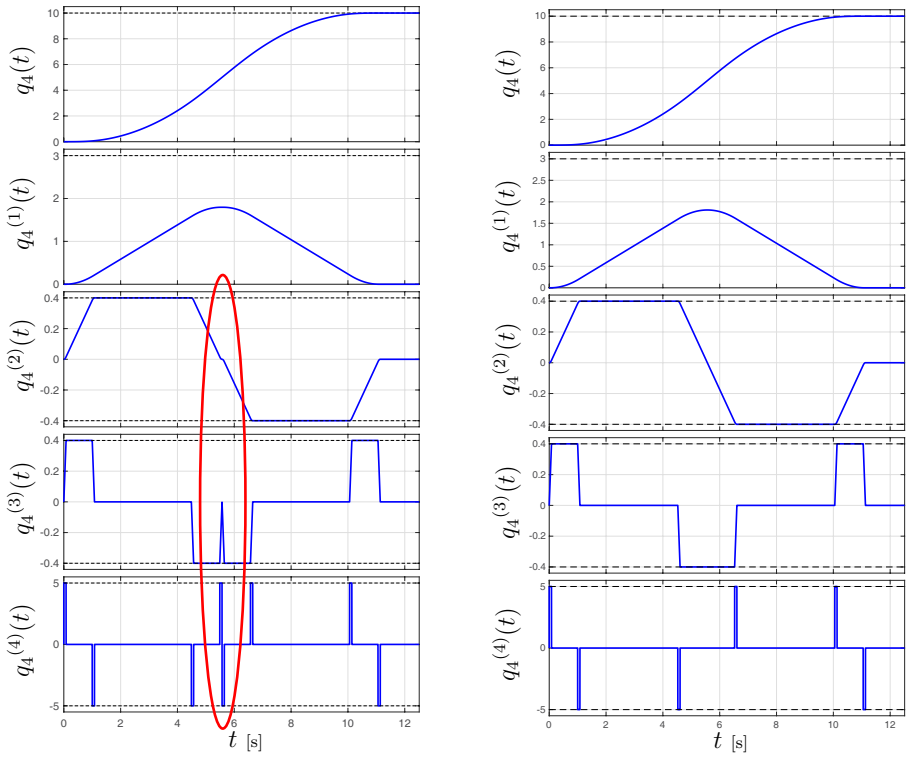

Figure 4: Profiles of the trajectory No. 1 obtained with a cascade of four rectangular smoothers with the parameters reported in Tab. 4 (a), compared with the profiles of the trajectory obtained by anticipating the deceleration phase (b). The red circle in figure (a) is used to highlight an apparently irregular behavior of the trajectory generator (discussed in the text) which has been removed in the trajectory of figure (b).

where for the sake of clarity the trajectory profiles of Fig. 3(b) have been reproduced, the lack of the constant velocity phase causes a fast oscillation of the jerk profile from its minimum value to zero and again to the minimum value. In order to avoid this oscillation and to further reduce the duration of the trajectory, the deceleration phase must be anticipated of a time period which exactly equals T_4. This means that T_1, that alone determines the duration of the acceleration and deceleration phases, must be reduced of

T_4. Since the maximum velocity is not reached, as a result the optimization procedure $T_1 = T_2 + T_3 + T_4$. Therefore, the anticipation simply requires that $T_1' = T_1 - T_4 = T_2 + T_3$. This can be obtained by modifying the procedure for kinematic optimization in Appendix A, which is based on (6), taking into account only three parameters at once, i.e.

$$\frac{T_i}{\alpha} \geq \alpha\, T_{i+1} + T_{i+2}, \qquad i = 1, \ldots, n-1. \tag{10}$$

This strategy is valid in general to avoid the above mentioned oscillation that may occurs in any derivative profile (and not only in the jerk) and leaded to the algorithm reported in Appendix B. By applying this method the trajectory of Fig. 4(b), characterized by

$$T_1 = 5.5249 \text{ s}, \;\; T_2 = 4.5249 \text{ s}, \;\; T_3 = 1 \text{ s}, \;\; T_4 = 0.08 \text{ s},$$

is obtained, for a total duration $T_{tot} = 11.1299$ s, that is -0.0743% of the duration of the multi-segment trajectory initially optimized. Even if the improvement is rather modest, this trajectory finally represents the rest-to-rest motion profile of shortest duration that can be obtained with the given set of constraints.

Similarly to trajectory No. 1, also for trajectory No. 2, the condition (3) with the initial parameters T_i is not satisfied for $i = 1$, and again by analyzing the trajectory profiles, which are reported in Fig. 5(a), it comes out that the velocity reaches and maintains for a certain interval a constant values lower than the given constraints. Furthermore, since $\min\{T_1, T_2\} < T_3 + T_4$, also the acceleration does not reach the given bound but only a constant value smaller than $q^{(2)}_{max}$. In this case, the optimization procedure modifies T_1, T_2 and T_3, leading to a trajectory whose first two derivatives do not reach the

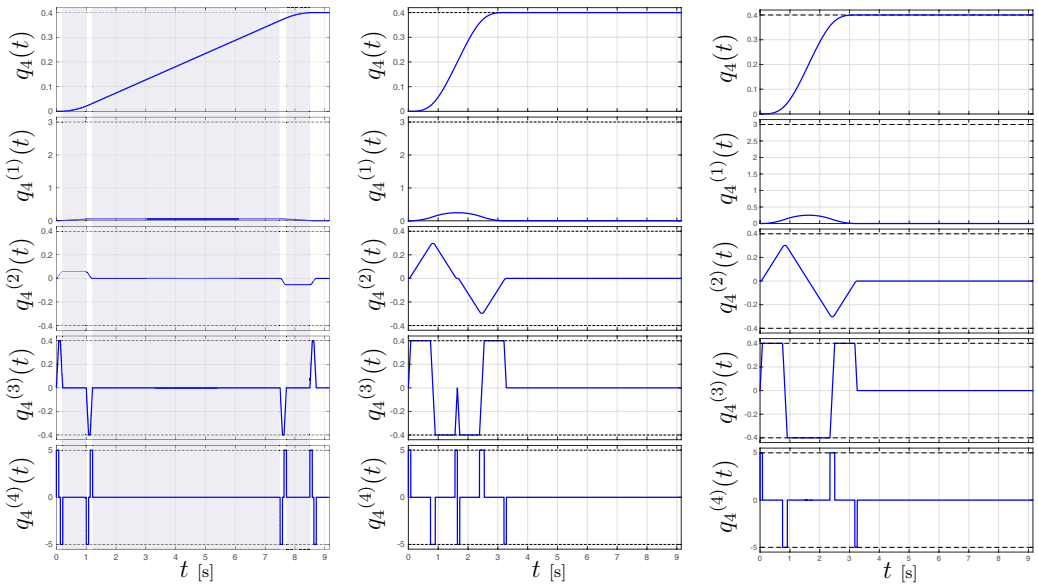

Figure 5: Profiles of position, velocity, acceleration, jerk and snap of the trajectories No. 2 obtained with a cascade of four rectangular smoothers with the parameters reported in Tab. 3 (a) and in Tab. 4 (b). In Figure (c) the trajectory obtained with the algorithm, reported in Appendix B, which eliminates the oscillation of the jerk is shown.

kinematic limits, which however cannot be reduced in duration since jerk or snap are always equal to their maximum allowed value. The reduction of the trajectory duration for the trajectory reported in Fig. 5(b) is -62.29%. Also in this case, it is possible to further reduce the duration of the trajectory, by eliminating the oscillation of the jerk in the middle of the trajectory with the procedure reported in Appendix B. The final motion profile, shown in Fig. 5(c), is characterized by the parameters

$$T_1 = 1.5887 \text{ s}, \;\; T_2 = 0.8344 \text{ s}, \;\; T_3 = 0.7544 \text{ s}, \;\; T_4 = 0.08 \text{ s},$$

and a duration of 3.2575 s (-0.8415% with respect to the trajectory already optimized according to the initial method).

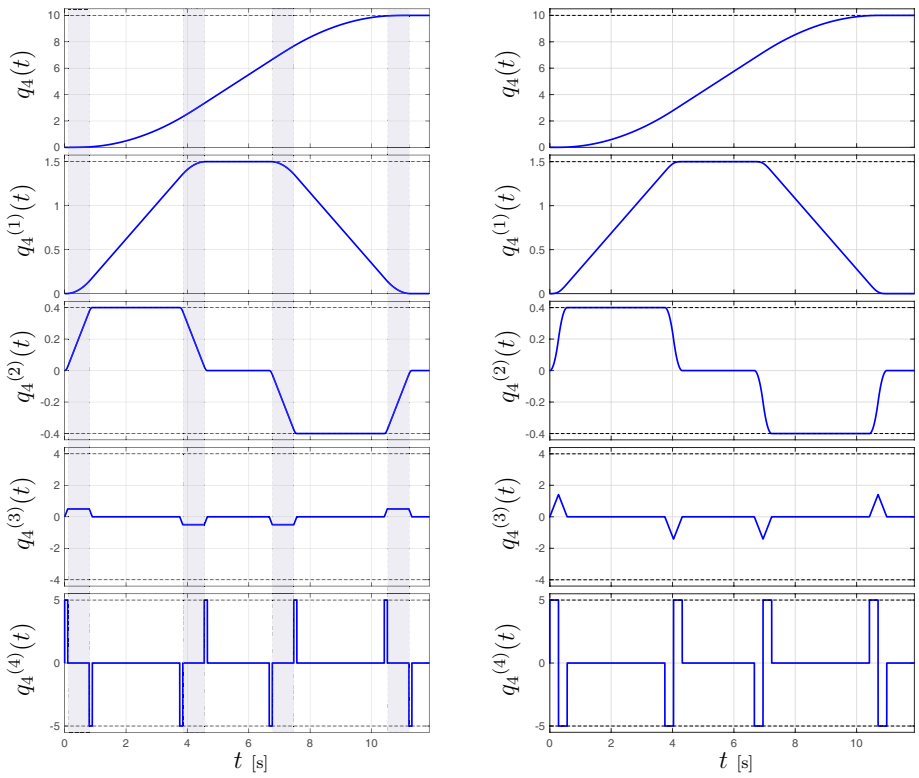

Figure 6: Profiles of position, velocity, acceleration, jerk and snap of the trajectories No. 3 obtained with a cascade of four rectangular smoothers with the parameters reported in Tab. 3 (a) and in Tab. 4 (b).

For the trajectory No. 3, shown in Fig. 6, the condition (3) is violated for $i = 3$, and accordingly the maximum jerk $q^{(3)}_{max}$ is not reached. The optimization procedure modifies the parameters that depends on $q^{(3)}_{max}$, i.e. T_3 and T_4. In this manner the duration of the trajectory is reduced by -2.95%, even if it is still compliant with all the constraints.

In the last example, the trajectory No. 4 is initially characterized by pa-

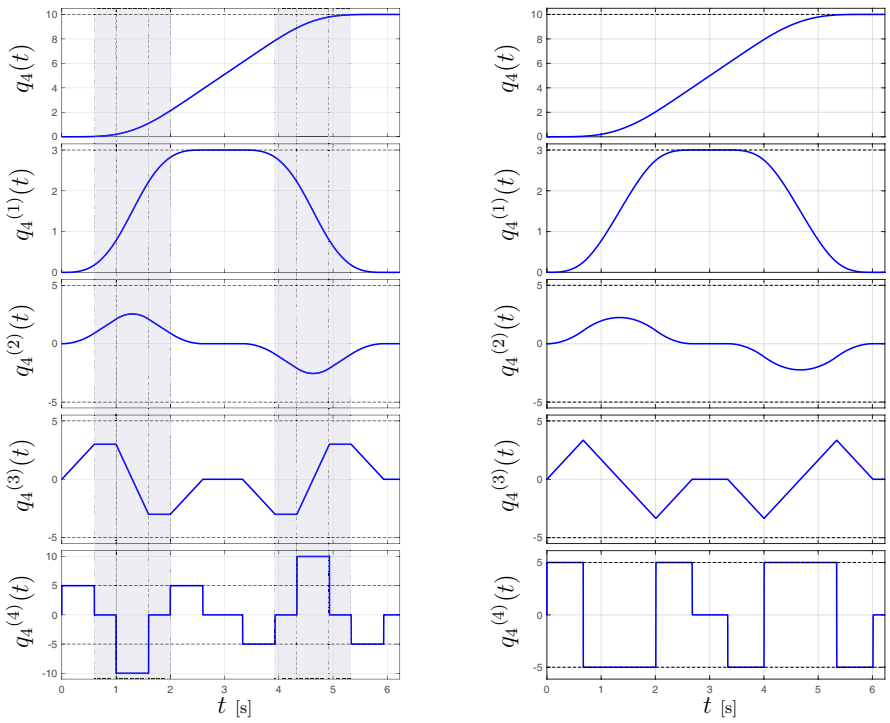

Figure 7: Profiles of position, velocity, acceleration, jerk and snap of the trajectories No. 4 obtained with a cascade of four rectangular smoothers with the parameters reported in Tab. 3 (a) and in Tab. 4 (b).

rameters T_i that do not satisfy (3) for $i = 3$. Moreover, $\min\{T_2, T_3\} < T_4$. Accordingly, both the jerk and the acceleration attain and maintain for a certain interval constant values smaller than the given bounds. Additionally, the snap profile overcomes the corresponding limit, see Fig. 7(a). The optimization procedure solves the three above mentioned problems, but in this case, the compliance with the given constraints requires a little increase of the trajectory duration (+1.31%). The final trajectory is shown in Fig. 7(b). Note that all the motion profiles are now compliant with the kinematic

bounds and that at each time instant one of them exactly equals the related limit. As a consequence the trajectory is time-optimal.
Note that in the last two examples the two algorithms for the kinematic optimization of the trajectories, which are reported in Appendix A and Appendix B respectively, provide exactly the same results.

5. Multi-segment polynomial trajectories with vibration suppression capabilities

Multi-segment trajectories are generally defined on the basis of a set of kinematic constraints. However, as shown in Biagiotti and Melchiorri (2012) the rectangular smoothers composing the proposed trajectory generator can be designed with the purpose of suppressing residual vibrations. In this way, it is possible to incorporate such a capability into the planned trajectory avoiding the use of further actions on the reference trajectory, like for instance the use of input shapers, which represent a sort of standard filtering technique for residual vibration suppression, see Singer and Seering (1990); Singhose et al. (1995); Singer et al. (1999).
In order to eliminate the oscillations caused by a poorly damped ($\delta \approx 0$) resonant mode at frequency $\omega_{n,i}$, it is sufficient to add to the trajectory generator a filter like (1) whose characteristic parameter is computed as

$$T_{\omega,i} = \frac{2\pi}{\omega_{n,i}}. \tag{11}$$

In this way, the frequency response of the filter assumes the shape shown in Fig. 8(a). In particular, its magnitude is null for $\omega = \omega_{n,i}$ and, accordingly, the filter does not excite the resonant mode at this frequency. In the same

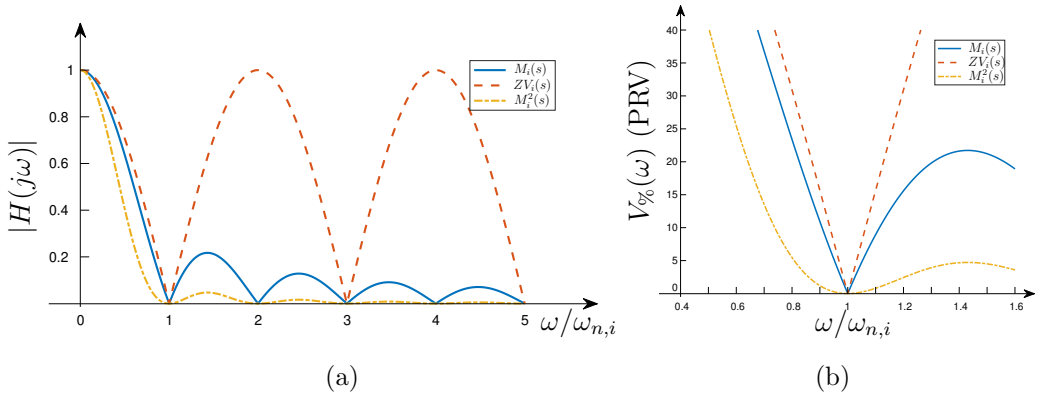

(a) (b)

Figure 8: Frequency response (a) and Percent residual vibration (b) of a rectangular smoother $M(s)$ compared with those of a Zero Vibration Input Shaper $ZV(s)$ and a double rectangular smoother $M^2(s)$, as a function of the normalized frequency $\omega/\hat{\omega}_n$.

figure, the frequency response of a Zero Vibration ($ZV_i(s)$) input shaper is reported, i.e. the simplest input shaper and, above all, the input shaper of minimum duration, $T_{zv,i} = \frac{\pi}{\omega_{n,i}}$. At a first glance, the main difference between the two filters is the low-pass characteristic of the rectangular smoother that allows it to reduce also the possible vibrations due to higher frequency modes. Note that, except for the a constant factor 100, the frequency response coincides with the sensitivity function of the filter with respect to variations of the resonant frequency of the plant, that is the Percent Residual Vibration (PRV) caused by the filter which is used to quantify its robustness [Kozak et al. (2006)]. From a close look of the PRV, shown in Fig. 8(b), it is evident that the rectangular smoother is more insensitive than the ZV Input shaper with respect to errors in the resonant frequency estimation. Moreover, the robustness of the proposed approach can be further enhanced by considering more than one smoother acting at the same frequency, see the PRV profile of $M_i^2(s)$ in Fig. 8(b).

In conclusion, to suppress the vibrations due to m resonant modes of the plant, the chain of filters composing the trajectory generator must include at least m filters, whose parameters $T_{\omega,i}$ are set according to (11).
In principle, a trajectory planner, that must take into account the kinematic constraints on the first n derivatives and the cancellation of the vibrations due to m oscillating modes, is composed by $n+m$ filters with a total duration

$$T_{tot} = \sum_{k=1}^{n} T_k + \sum_{k=1}^{m} T_{\omega,k}.$$

However, as a side effect the filters for vibration suppression cause limitations on the derivatives of the trajectory and consequently some of the filters initially designed to meet the kinematic constraints can become redundant. For this reason a procedure for taking into account only the filters that are strictly necessary to comply with all the constraints must be devised. With this respect, it is worth noticing that the m filters characterized by the time constant $T_{\omega,i}$ computed with (11) are mandatory to obtain an ideal vibrations suppression, while some of the n filters computed according to the kinematics constraints can be omitted, with a consequent reduction of the total trajectory duration. In particular, by solving (2) with respect to $q_{max}^{(i)}$, it is possible to deduce the relation

$$q_{max}^{(i)} = \frac{|h|}{\prod_{k=1}^{i} T_k}, \qquad i = 1, \ldots, n \tag{12}$$

leading to the conclusion that, by increasing the value of a generic parameter T_i computed according to (2), the peak values reached by the derivatives of the trajectory obtained with a displacement h are simply reduced and,

therefore, they are still compliant with the given limits.

A simple way for detecting which filters are unnecessary consists in checking if for any elements T_i, $i = 1, \ldots, n$, resulting from the kinematic constraints there exists an element of $T_{\omega,i}$, $i = 1, \ldots, m$ larger in magnitude, i.e. $T_p \leq T_{\omega,q}$. In this case, it is possible to substitute the parameter T_p with $T_{\omega,q}$ without violating the kinematic constraints. A systematic way to perform this operation starts from the vectors $\boldsymbol{T} = [T_i]$ and $\boldsymbol{T}_\omega = [T_{\omega,i}]$ sorted in descendent order. Then, the algorithm reported in the flowchart of Fig. 9 can be applied in order to determine the vector $\boldsymbol{T}^\star$ composed by l elements, with $l \leq n + m$. The number l represents the minimum number of filters composing the trajectory generator that complies with the all the constraints (2) and (11), and the elements of $\boldsymbol{T}^\star$ are the parameters that must be imposed to these filters. The Matlab code of the function implementing this algorithm is reported in Appendix C.

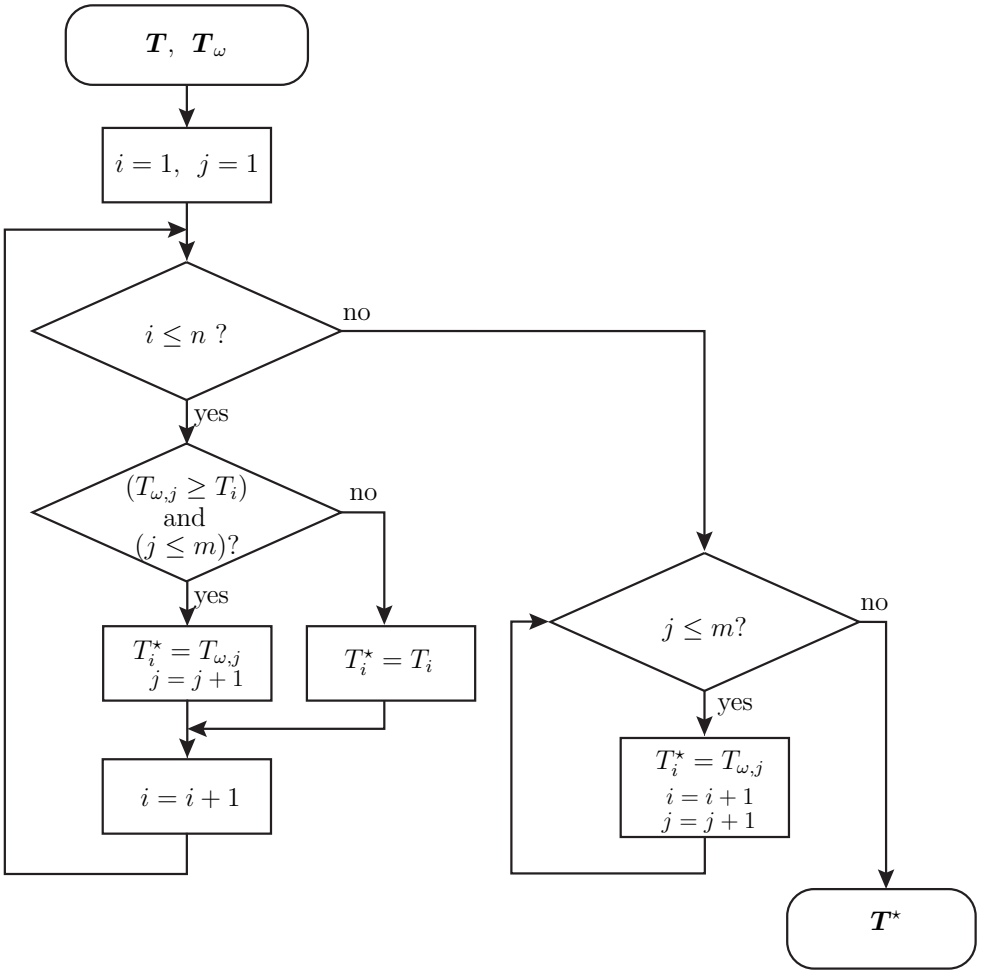

Figure 9: Algorithm for the minimization of the number of filters of a trajectory generator compliant with the constraints (2) and (11).

6. Experimental validation of the optimization procedure of trajectories with kinematic and frequency constraints

6.1. Description of the experimental setup

In order to validate the proposed method and show its advantages the experimental setup of Fig. 10 has been used. It is based on a thin stainless

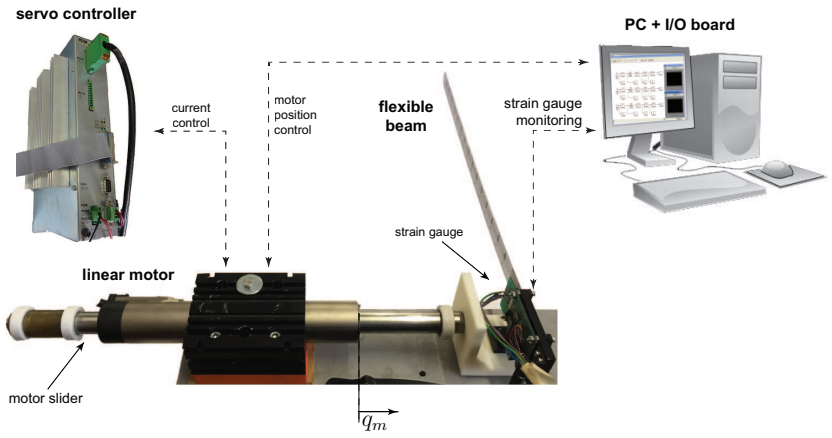

Figure 10: Experimental setup based on a flexible link.

steel flexible link directly connected to the slider of a linear motor. The side of the link connected to the motor is instrumented with a strain gauge that detects the local deformation of the beam. The position control of the motor and the trajectory generation are performed by a standard PC with a Pentium IV 3 GHz processor equipped with a Sensoray 626 data acquisition board and running the RTAI-Linux operating system, which guarantees a sampling time $T_s = 0.0005$ s. The discrete-time implementation of the filters is reported in Biagiotti and Melchiorri (2012).

The plant can be modeled as in Fig. 11. The dynamics of the link subject to the lateral acceleration $\ddot{x}$ of the motor is described by a partial differential equation [Luo et al. (1995)]. The assumption of separability of spatial and temporal variables allows to obtain a closed-form solution of the bending deformation

$$w(y,t) = \sum_{i=1}^{\infty} \psi_i(y)\, q_i(t) \tag{13}$$

where $\psi_i(y)$ are the mode shapes depending on the boundary conditions imposed by the physical system, and $q_i(t)$ are the generalized modal coordinates,

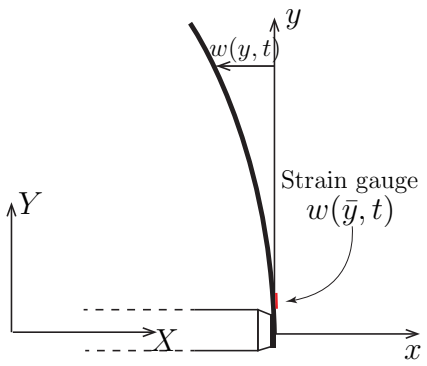

Figure 11: Model of the uniform cantilever beam used in the experiments.

oscillatory in time according to the frequency ω_i [Kane et al. (1987); Bellezza et al. (1990)]. Even if the expression (13) takes into account infinite terms, in practice only few modes are meaningful for the bending of the beam. In particular, the flexible link used in the experiments is strongly affected by two modes located at $\omega_{r1} \approx 20.18$ rad/s and $\omega_{r2} \approx 127.5$ rad/s, respectively, while additional contributions are negligible. The dynamic modes are both slightly damped. For instance, the fist mode is characterized by a damping coefficient $\delta = 0.0043$. For this reason, it is possible to design the filters, both the smoothers and the input shapers, by assuming $\delta \approx 0$.

The strain gauge, sensing the deflection in a specific point of the beam, provides a signal $V_w(t)$ proportional to $w(\bar{y}, t)$ that is therefore a linear combination of the temporal modes according to the constant coefficients $\psi_i(\bar{y})$. In order to quantify the level of vibrations, the output voltage $V_w(t)$ of the strain gauge is directly used, see Fig. 12. Finally, with regard to Fig. 12, it is worth remarking that, within the given kinematic limits, the linear actuator, represented as a simple saturation, is supposed to be able to "perfectly" track the reference trajectory produced by the chain of filters, i.e. $q_n(t) \approx q_n^\star(t)$.

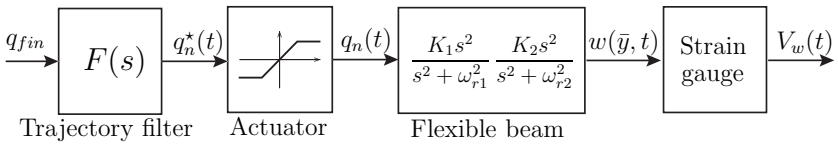

Figure 12: Block-scheme representation of the experimental setup, based on a flexible link, shown in Fig. 10.

6.2. Experiments

In the first example, the following specifications have been considered:

$$h = 0.03 \text{ m}, \quad q_{max}^{(1)} = 0.1 \text{ m/s}, \quad q_{max}^{(2)} = 1 \text{ m/s}^2. \tag{14}$$

Accordingly, the parameters of the two smoothers that generate the second order optimal trajectory compliant with the given constraints, computed according to the technique illustrated in Sections 2 and 3, are $T_1 = 0.3$ s, $T_2 = 0.1$ s ($T_{tot} = 0.4$ s). The initial motion profile is shown in Fig. 13 in black color. Its application to the experimental setup produces in the flexible link a certain level of vibrations, measured by the voltage signal $V_w(t)$ of the strain gauge, see Fig. 14(a). Since signal $V_w(t)$ is affected by a high level of noise, an analysis in the frequency domain has been performed, by applying a Fast Fourier Transform (FFT) to the samples of $V_w(t)$ measured after the end of the motion. The spectrum $|V_w(j\omega)|$ in the frequency range of interest is shown in Fig. 14(b), where it is compared with the frequency response of the chain of filters used to plan the reference trajectory. Note that the signal exhibits a peak value at the frequency ω_{r1}, that corresponds to the residual vibration tied to the first resonant mode, while the contribution of the second mode is not appreciable. It is also worth noticing that the

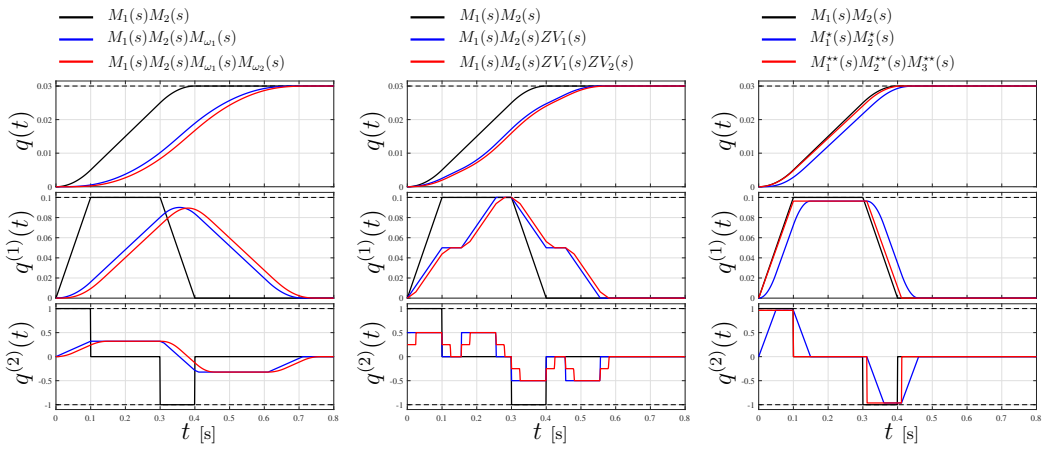

Figure 13: Profiles of position, velocity and acceleration of the trajectory used in the first test on the flexible link. In all the figures, the solid black line denotes the initial trajectory. Additional smoothers for vibration reduction are considered in (a), input shapers in (b) and the optimization procedure proposed in Sec. 5 in (c).

frequency spectrum of the trajectory generator has a zero very close to ω_{r1}.

In order to highlight the advantages of the proposed optimization procedure, several techniques, aiming at a reduction of the residual vibration, have been compared. In particular, the following approaches have been tested.

(a) A smoother $M_{\omega,1}(s)$ with $T_{\omega_1} = \frac{2\pi}{\omega_{r1}} = 0.3114$ s is simply added to the initial chain (accordingly the duration of the trajectory becomes $T_{tot} = T_1 + T_2 + T_{\omega,1} = 0.7114$ s, that is +77.85% with respect to its initial value). The resulting trajectory is shown in Fig. 13(a) (blue line).

(b) A second smoother $M_{\omega,2}(s)$ with $T_{\omega_2} = \frac{2\pi}{\omega_{r2}} = 0.0493$ s is added to the chain including $M_{\omega,1}(s)$ ($T_{tot} = T_1 + T_2 + T_{\omega_1} + T_{\omega_2} = 0.7606$ s,

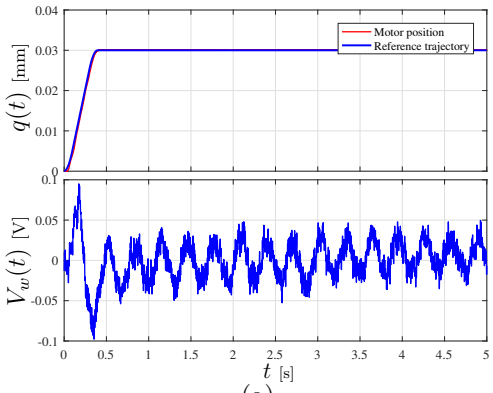

(a)

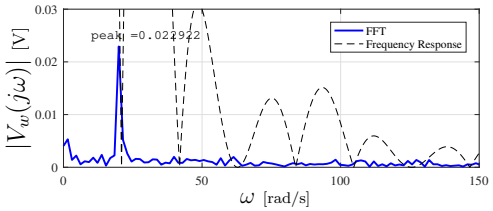

(b)

Figure 14: Initial motion profile, based on kinematic constraints (14), applied to the flexible link in the first experiment and measurement of the link deflection via the strain gauge (a). Magnitude of the frequency spectrum of the strain gauge output signals $V_w(t)$ and comparison with the frequency response of the trajectory generator (b).

+90.15%). The resulting trajectory is shown in Fig. 13(a) (red line).

(c) An input shaper $ZV_1(s)$ with $T_{zv1} = \frac{\pi}{\omega_{r1}} = 0.1557$ s is used in lie of the smoother after the chain $M_1(s)M_2(s)$ ($T_{tot} = T_1 + T_2 + T_{zv1} = 0.5557$ s, +38.92%). The resulting trajectory is shown in Fig. 13(b) (blue line).

(d) A second input shaper $ZV_2(s)$ with $T_{zv2} = \frac{\pi}{\omega_{r2}} = 0.0246$ s is considered ($T_{tot} = T_1 + T_2 + T_{zv1} + T_{zv2} = 0.5803$ s, +45.07%). The resulting trajectory is shown in Fig. 13(b) (red line).

(e) The optimization procedure proposed in Sec. 5 is applied to the chain

of smoothers composed by $M_1(s)M_2(s)$ and $M_{\omega,1}(s)$ obtaining a filter of the second order $M_1^\star(s)M_2^\star(s)$ with $T_1^\star = T_{\omega_1}$ and $T_2^\star = T_2$ ($T_{tot} = 0.4114$ s, $+2.85\%$), therefore $M_1^\star(s)M_2^\star(s) = M_{\omega,1}(s)M_2(s)$. The resulting trajectory is shown in Fig. 13(c) (blue line).

(f) The optimization procedure is applied to the chain of smoothers composed by $M_1(s)M_2(s)$ and $M_{\omega,1}(s)M_{\omega,2}(s)$ obtaining a third order filter $M_1^{\star\star}(s)M_2^{\star\star}(s)M_3^{\star\star}(s)$ with $T_1^{\star\star} = T_{\omega_1}$, $T_2^{\star\star} = T_2$ and $T_3^{\star\star} = T_{\omega_2}$ ($T_{tot} = 0.4606$ s, $+15.15\%$), i.e. $M_1^{\star\star}(s)M_2^{\star\star}(s)M_3^{\star\star}(s) = M_{\omega,1}(s)M_2(s)M_{\omega,2}(s)$. The resulting trajectory is shown in Fig. 13(c) (red line).

The original trajectory is modified by the above methods as shown in Fig. 13. The kinematic constraints are met in any case. The additional smoothers increase the continuity level of the motion profile, see Fig. 13(a), while with the input shapers the continuity level remains unchanged, see Fig. 13(b). The optimization procedure leads to a trajectory generator whose order is not smaller than the order of the initial filter only based on the kinematic constraints. The major advantage of the optimization procedure is the little increment of the trajectory duration, if compared with the insertion of additional elements, either smoothers or input shapers, for vibration suppression. As regard as the effectiveness of the different methods in vibration reduction, the results are illustrated in Fig. 15 in the time domain and in Fig. 16 in the frequency domain. In particular, the FFT analysis shows that the vibration levels obtained by the different methods are similar. As a matter of fact, the magnitude of the frequency component at ω_{r1} is 0.0098552 (-57.00% of the initial value) in case (a), 0.0075938 (-66.87%) in case (b), 0.010274 (-55.18%) in case (c), 0.010076 (-56.04%) in case (d), 0.010816 (-52.81%)

in case (e), 0.010257 (-55.25%) in case (f). The first filter designed on the basis of ω_{r1} leads to a reduction of the residual vibration of about 50%, while the application of the second filter slightly influences the level of vibration at ω_{r1}. In general, the three different approaches are equivalent, but the very limited increase in duration of the trajectory based on the optimized combination of kinematic and frequency constraints makes this technique highly preferable.

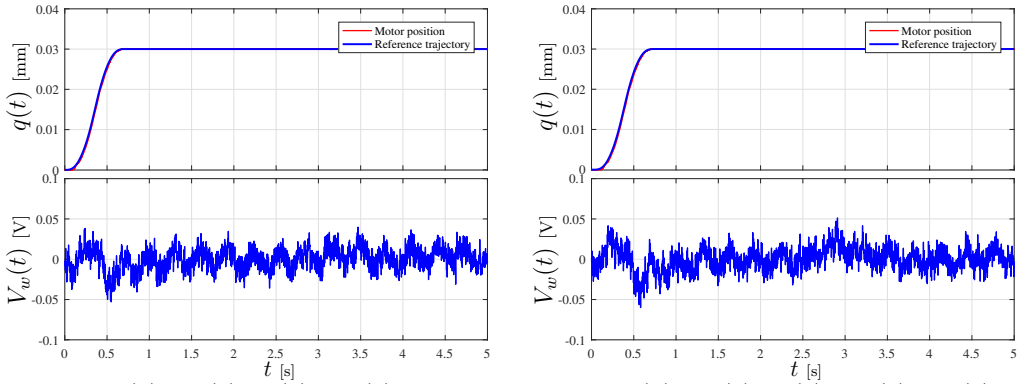

(a) $M_1(s)M_2(s)M_{\omega_1}(s)$

(b) $M_1(s)M_2(s)M_{\omega_1}(s)M_{\omega_2}(s)$

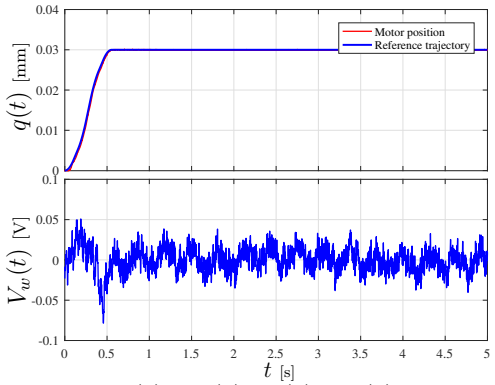

(c) $M_1(s)M_2(s)ZV_1(s)$

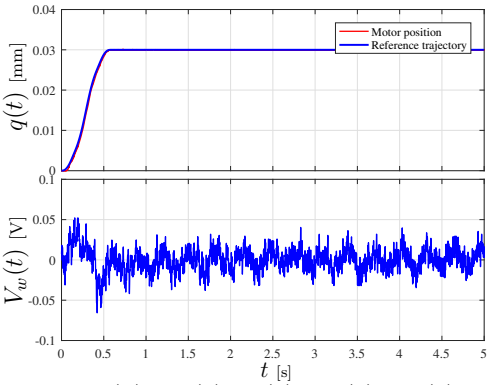

(d) $M_1(s)M_2(s)ZV_1(s)ZV_2(s)$

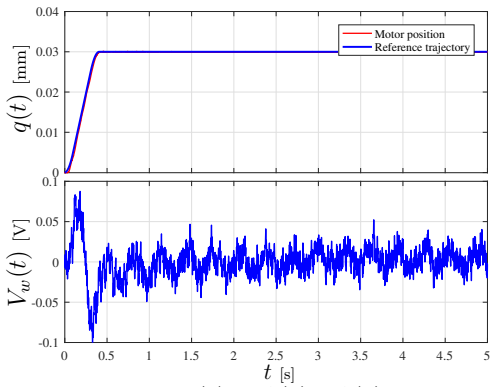

(e) $M_1^{\star}(s)M_2^{\star}(s)$

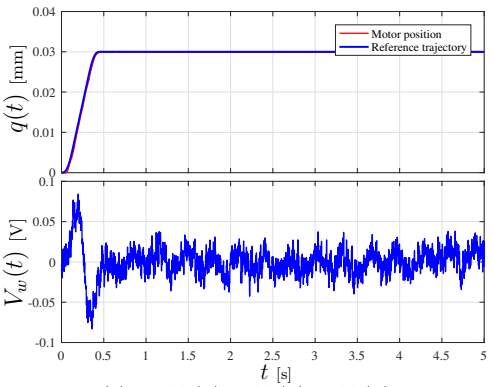

(f) $M_1^{\star\star}(s)M_2^{\star\star}(s)M_3^{\star\star}(s)$

Figure 15: Motions applied to the flexible link in the first test and measurement $V_w(t)$ of the produced vibrations. The letters denoting the different subfigures are consistent with the list in the text.

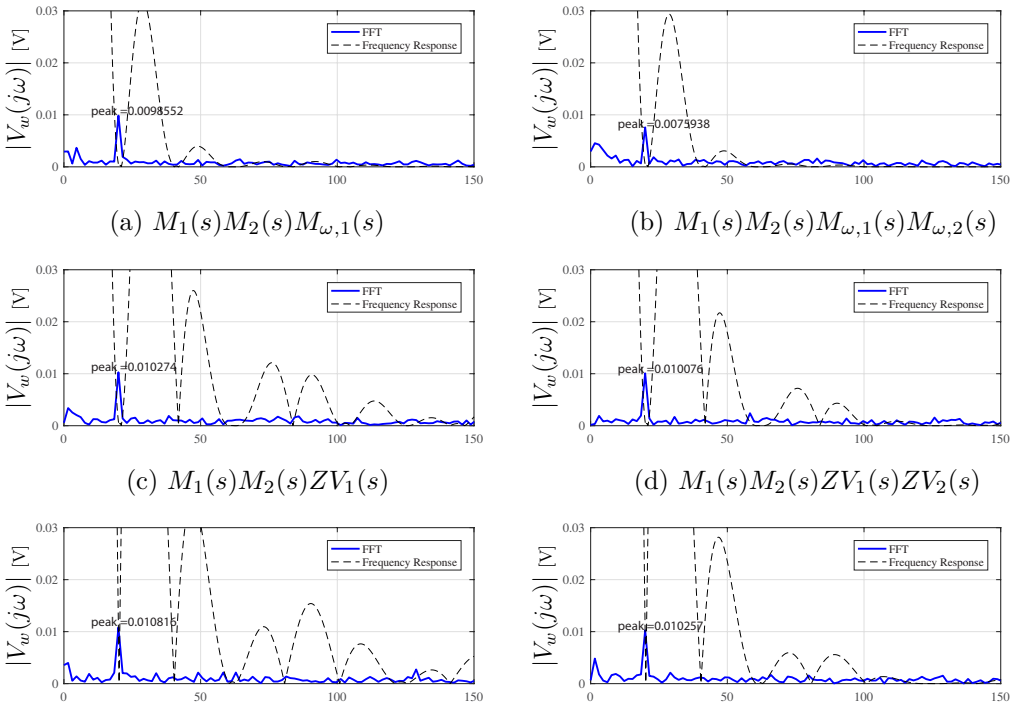

(a) $M_1(s)M_2(s)M_{\omega,1}(s)$ (b) $M_1(s)M_2(s)M_{\omega,1}(s)M_{\omega,2}(s)$

(c) $M_1(s)M_2(s)ZV_1(s)$ (d) $M_1(s)M_2(s)ZV_1(s)ZV_2(s)$

(e) $M_1^\star(s)M_2^\star(s)$ (f) $M_1^{\star\star}(s)M_2^{\star\star}(s)M_3^{\star\star}(s)$

Figure 16: Magnitude of the frequency spectrum of the strain gauge output signals $V_w(t)$ reported in Fig. 15 and comparison with the frequency response of the filters generating the reference position.

In a second experiment, a third order trajectory filter, compliant with the specifications

$$h = 0.04 \text{ m}, \quad q_{max}^{(1)} = 0.1 \text{ m/s}, \quad q_{max}^{(2)} = 0.5 \text{ m/s}^2, \quad q_{max}^{(3)} = 12 \text{ m/s}^3, \quad (15)$$

is initially considered. The parameters of the three smoothers composing the trajectory generator are $T_1 = 0.4$ s, $T_2 = 0.2$ s and $T_3 = 0.0417$ s ($T_{tot} = 0.6417$ s).

The original motion profile and the measurement of the produced residual vibrations are shown in Fig. 17 and Fig. 18, respectively. Note that, despite the higher order of the trajectory, the level of vibrations is greater than the level obtained in the first experiment. This effect can be explained by considering the frequency response of the trajectory filter, reported in Fig. 18(b), whose magnitude is rather large in the range of frequencies centered around ω_{r1}. Moreover, the initial motion profile considered in this experiment, tends to excite also the resonant mode at ω_{n2}, as highlighted by the frequency analysis in Fig. 18(b).

The same tests performed in the first experiment have been repeated starting from this different trajectory. Besides the different structure of the initial trajectory filter (composed by three smoothers) and the different parameters values, the main difference with respect to the first experiment concerns the result of the optimization procedure. In case (e), the optimal filter is composed by three smoothers $M_1^\star(s)M_2^\star(s)M_3^\star(s)$ characterized by $T_1^\star = T_1 = 0.4$ s, $T_2^\star = T_{\omega_1} = 0.3114$ s and $T_3^\star = T_3 = 0.0417$ s, i.e. $M_1^\star(s)M_2^\star(s)M_3^\star(s) = M_1(s)M_{\omega,1}(s)M_3(s)$. In case (f), the optimal filter is again a combination of three smoothers $M_1^{\star\star}(s)M_2^{\star\star}(s)M_3^{\star\star}(s)$, whose parameters are $T_1^{\star\star} = T_1 = 0.4$ s, $T_2^{\star\star} = T_{\omega_1} = 0.3114$ s and $T_3^{\star\star} = T_{\omega_2} = 0.0493$ s,

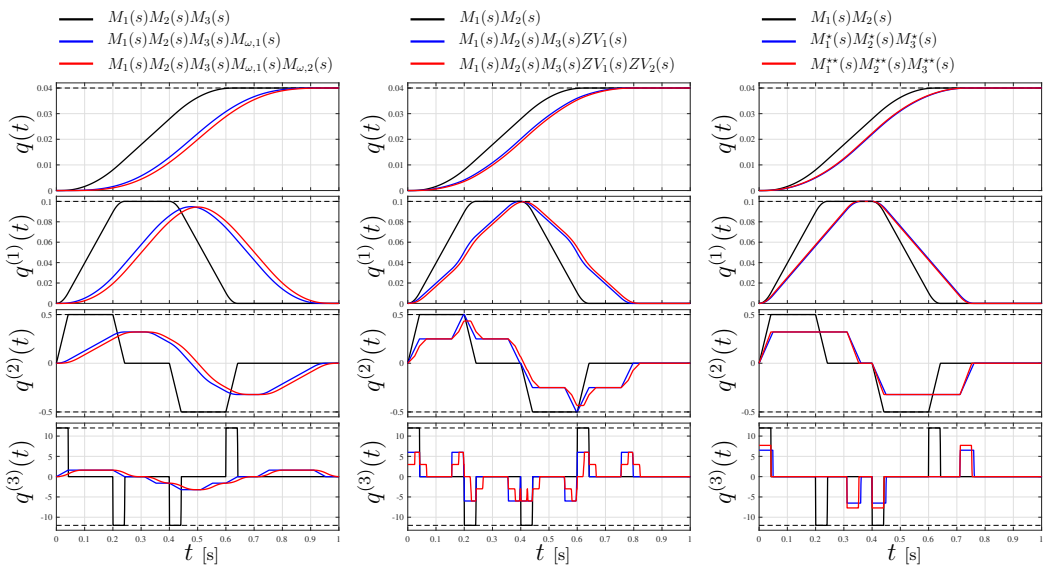

(a) (b) (c)

Figure 17: Profiles of position, velocity and acceleration of the trajectory used in the second test on the flexible link. In all the figures, the solid black line denotes the initial trajectory. Additional smoothers for vibration reduction are considered in (a), input shapers in (b) and the optimization procedure proposed in Sec. 5 in (c).

i.e. $M_1^\star(s)M_2^\star(s)M_3^\star(s) = M_1(s)M_{\omega,1}(s)M_{\omega,2}(s)$.

The motion profiles, achieved with the different techniques, are shown in Fig. 17, proving that the given kinematic constraints are still met. The residual vibrations produced in the flexible link by each motion profile are shown in Fig. 18, and then analyzed in the frequency domain, see Fig. 20. Table 5 summarizes the achieved results in terms of both trajectory duration and residual vibrations reduction. In both cases the percentage variation with respect to the original trajectory is computed.

Like in the first experiment, the different filtering techniques show simi-

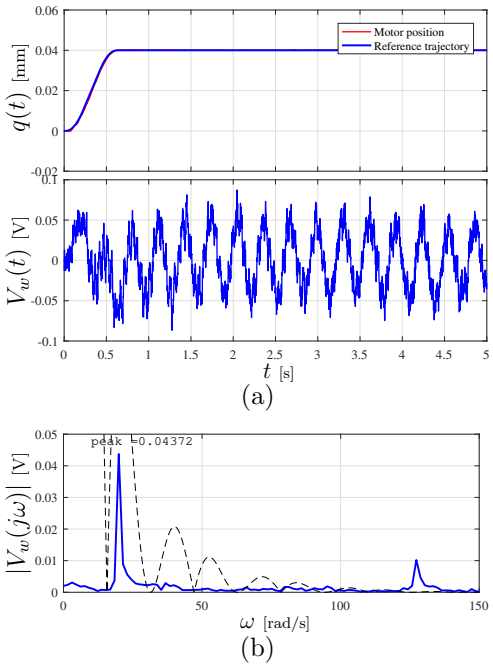

Figure 18: Initial motion profile, based on kinematic constraints (15), applied to the flexible link in the second experiment and measurement of the link deflection via the strain gauge (a). Magnitude of the frequency spectrum of the strain gauge output signals $V_w(t)$ and comparison with the frequency response of the trajectory generator (b).

lar performances in terms of vibrations reduction. Note that the first filter, based on ω_{r1}, also contributes to reduce the residual vibrations at ω_{r2}, while the second one, which is tuned by considering ω_{r2}, slightly improves the vibration suppression at ω_{r1}.

The proposed optimization procedure based on a proper combination of rectangular smoothers is characterized by the shortest duration among the tested methods, leading to the conclusion that an integrated design of the trajectory planner, taking into account both the kinematic limits imposed by the actuator/application and the resonant frequencies of the plant, provides the

	(a)	(b)	(c)	(d)	(e)	(f)
T_{tot} [s]	0.9530	1.0023	0.7973	0.8220	0.7530	0.7606
$\Delta T_{tot}\%$	48.52	56.20	24.25	28.10	17.35	18.53
V [mV]	22.278	13.744	21.143	14.649	18.536	15.851
$\Delta V\%$	-49.04	-68.56	-51.64	-66.49	-57.60	-63.74

Table 5: Duration and residual vibration level associated with the different trajectory filters obtained by modifying the original generator based on the kinematic constraints (15). Symbol V denotes the magnitude of the spectral component at ω_{r1}.

best results in terms of motion duration and residual vibration reduction.

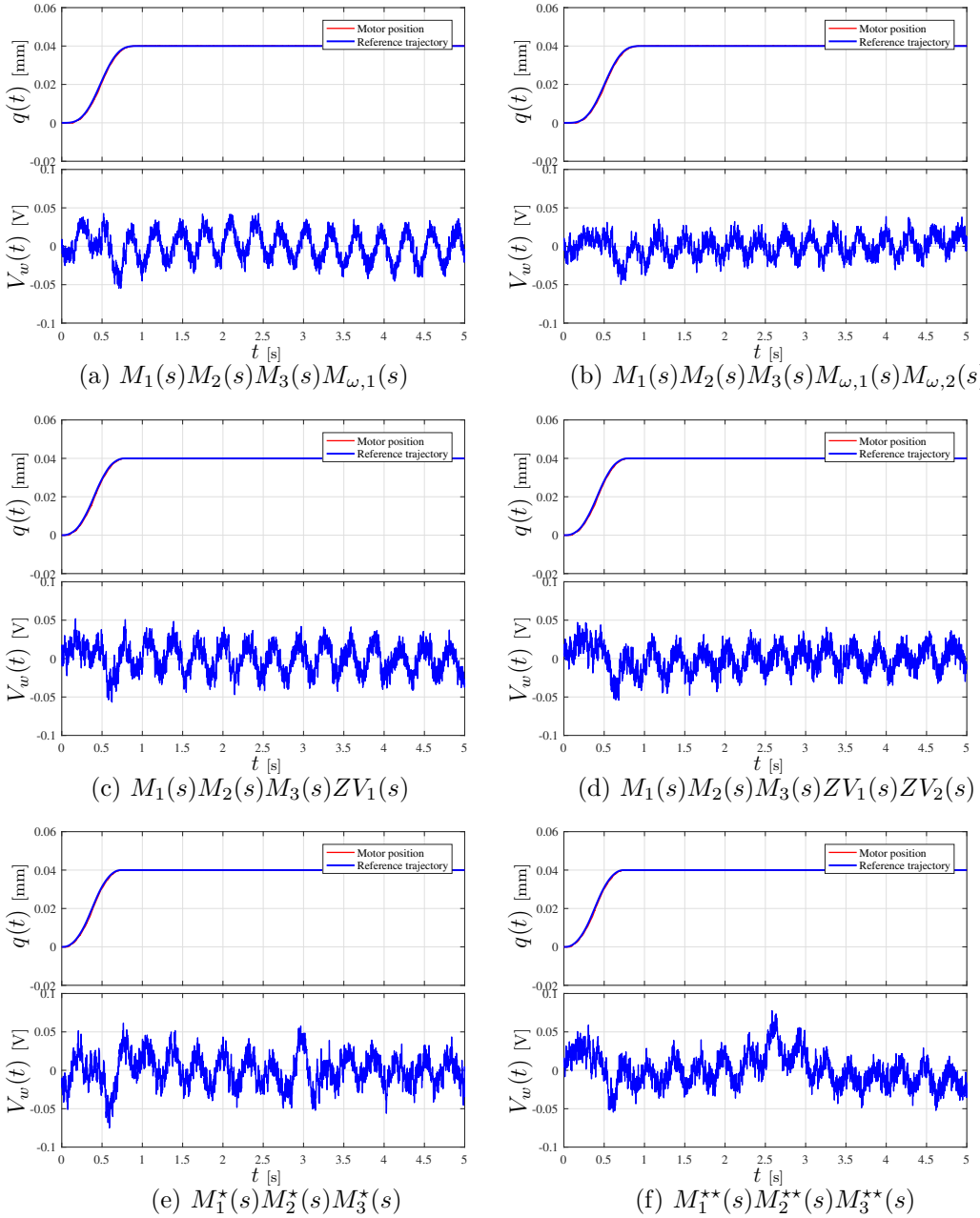

(a) $M_1(s)M_2(s)M_3(s)M_{\omega,1}(s)$ (b) $M_1(s)M_2(s)M_3(s)M_{\omega,1}(s)M_{\omega,2}(s)$

(c) $M_1(s)M_2(s)M_3(s)ZV_1(s)$ (d) $M_1(s)M_2(s)M_3(s)ZV_1(s)ZV_2(s)$

(e) $M_1^{\star}(s)M_2^{\star}(s)M_3^{\star}(s)$ (f) $M_1^{\star\star}(s)M_2^{\star\star}(s)M_3^{\star\star}(s)$

Figure 19: Motions applied to the flexible link in the second experimental test and measurement $V_w(t)$ of the produced vibrations.

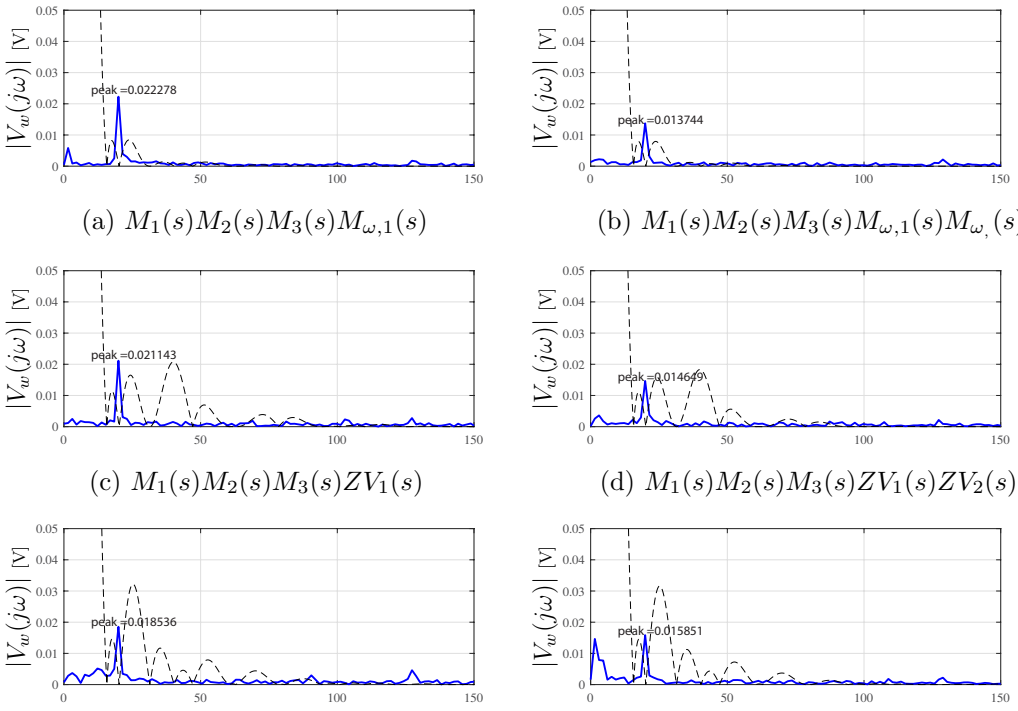

(a) $M_1(s)M_2(s)M_3(s)M_{\omega,1}(s)$ (b) $M_1(s)M_2(s)M_3(s)M_{\omega,1}(s)M_{\omega,}(s)$

(c) $M_1(s)M_2(s)M_3(s)ZV_1(s)$ (d) $M_1(s)M_2(s)M_3(s)ZV_1(s)ZV_2(s)$

(e) $M_1^\star(s)M_2^\star(s)M_3^\star(s)$ (f) $M_1^{\star\star}(s)M_2^{\star\star}(s)M_3^{\star\star}(s)$

Figure 20: Magnitude of the frequency spectrum of the strain gauge output signals $V_w(t)$ reported in Fig. 18 and comparison with the frequency response of the filters generating the reference position.

7. Conclusions

In this paper, a complete framework for the (online) generation of optimal rest-to-rest trajectories subject to kinematic and frequency constraints is presented. The key point of the proposed approach is the use of a chain of rectangular smoothers for the design of computationally efficient trajectory planners of any order. Several attempts of designing generic n-th order trajectories of minimum duration under kinematic constraints have been proposed in the literature but, to the best of our knowledge, only the use of smoothers together with the tools proposed in this paper for the calculation of their parameters allow (for the first time) a true optimization of the trajectory, even if limited to the rest-to-rest case.

Additionally, a second procedure allows to minimize the trajectory duration when also frequency specifications, tied to the suppression of residual vibrations, are considered. The experimental tests confirm that the integrated design of the trajectory leads to a duration of the motion considerably smaller than the simple application of filtering techniques, like input shapers, to the initial trajectory compliant with the kinematic bounds. On the other hand, the capability of the optimized trajectory of reducing the residual vibrations are similar to the use of an additional filter.

Appendix A. Procedure for the verification and optimization of parameters $\boldsymbol{T_i}$

The following is an example implementation in the Matlab programming language of the algorithm of Fig. 2 for the optimization of parameters T_i,

$i = 1, \ldots, n$ defining the n-th order multi-segment trajectory of minimum duration under kinematic constraints.

```
function [ Tout ] = CheckConstraintsT(Tin)
amax = 0.999999;
amin = 0.95;
n = length(Tin);
Tout=Tin;
for i=n-1:-1:1
      if Tout(i)< sum(Tout(i+1:end))
        a = -sum(Tout(i+2:end))/2/Tout(i+1)+sqrt((sum(Tout(i+2:end))/2/Tout(i+1))^2+Tout
            (i)/Tout(i+1));
        a = min([max([a amin]), amax]);
        Tout(i) = Tout(i)/a;
        Tout(i+1) = Tout(i+1)*a;
        Tout  = CheckConstraintsT(Tout);
     end
end
end
```

The input vector `Tin` contains the initial guess of the parameters T_i computed according to (2), while `Tout` is the vector of the optimal parameters.

Appendix B. Procedure for the optimization of parameters T_i avoiding unwanted oscillations in the trajectory profiles

Matlab function for the optimization of parameters T_i, $i = 1, \ldots, n$ defining the n-th order multi-segment trajectory of minimum duration under kinematic constraints that solves the problem of unwanted oscillations of trajectory derivatives from their max/min value to zero and again to the max/min value (see example in Fig. 4).

```
function [ Tout ] = CheckConstraintsT1( Tin )
amax = 0.999999;
amin = 0.95;
n = length(Tin);
Tout=Tin;
if ( Tout(n-1) < Tout(n) )
    Tout(n) = sqrt(Tout(n-1)*Tout(n));
    Tout(n-1) = Tout(n);
end
for i=n-2:-1:1
```

```
            if ( Tout(i)< Tout(i+1) + Tout(i+2) )
              a =-Tout(i+2)/2/Tout(i+1)+sqrt((Tout(i+2)/2/Tout(i+1))^2+Tout(i)/Tout(i+1));
              a = min([max([a amin]), amax]);
              Tout(i) = Tout(i)/a;
              Tout(i+1) = Tout(i+1)*a;
              Tout  = CheckConstraintsT1( Tout );
            end
end
end
```

The input vector `Tin` contains the initial guess of the parameters T_i computed according to (2), while `Tout` is the vector of the optimal parameters.
This function has been used in the Matlab/Simulink toolbox mentioned in the introduction (see Biagiotti (2019)) for the automatic design of trajectory generators compliant with kinematic and frequency constraints.

Appendix C. Procedure for the optimization of a trajectory under kinematic and frequency constraints

Implementation in the Matlab programming language of the algorithm of Fig. 9 for the optimization of the number of filters, and the related parameters, defining a multi-segment trajectory of minimum duration compliant with n kinematic constraints and m frequency constraints.

```
function [Tstar] = MergeConstraintsT( T, Tw )
n = length(T);
m = length(Tw);
j = 1;
Tstar = [];
for i = 1: n
        if (j <= m) & (Tw(j) >= T(i))
            Tstar(i) = Tw(j);
            j = j + 1;
        else
            Tstar(i) = T(i);
        end
end
Tstar = [Tstar Tw(j:end)];
```

The input vectors `T` and `Tw` contain the parameter T_i computed according to the kinematic constraints and the parameters $T_{\omega,i}$ obtained with (11). The output vector `Tstar` is composed by the minimum number of parameters that allow the trajectory to be compliant with all the initial constraints.

References

Bellezza, F., Lanari, L., Ulivi, G., 1990. Exact modeling of the flexible slewing link, in: Proceedings., IEEE International Conference on Robotics and Automation, pp. 734–739.

Besset, P., Bearee, R., 2017. Fir filter-based online jerk-constrained trajectory generation. Control Engineering Practice 66, 169 – 180.

Biagiotti, L., 2019. Automatic design of an optimal trajectory generator in matlab/simulink. URL: `http://www.dii.unimore.it/~lbiagiotti/BuildTrajectoryGenerator.zip`.

Biagiotti, L., Melchiorri, C., 2008. Trajectory Planning for Automatic Machines and Robots. Springer Berlin Heidelberg.

Biagiotti, L., Melchiorri, C., 2011. Input shaping via b-spline filters for 3-d trajectory planning, in: 2011 IEEE/RSJ International Conference on Intelligent Robots and Systems, pp. 3899–3904.

Biagiotti, L., Melchiorri, C., 2012. Fir filters for online trajectory planning with time- and frequency-domain specifications. Control Engineering Practice 20, 1385 – 1399.

Biagiotti, L., Melchiorri, C., 2013. Online trajectory planning and filtering for

robotic applications via b-spline smoothing filters, in: 2013 IEEE/RSJ International Conference on Intelligent Robots and Systems, pp. 5668–5673.

Biagiotti, L., Zanasi, R., 2010. Time-optimal regulation of a chain of integrators with saturated input and internal variables: an application to trajectory planning. IFAC Proceedings Volumes 43.

Bianco, C.G.L., Ghilardelli, F., 2014. A discrete-time filter for the generation of signals with asymmetric and variable bounds on velocity, acceleration, and jerk. IEEE Transactions on Industrial Electronics 61, 4115–4125.

Chen, C.S., Lee, A.C., 1998. Design of acceleration/deceleration profiles in motion control based on digital fir filters. International Journal of Machine Tools and Manufacture 38, 799 – 825.

Erkorkmaz, K., Altintas, Y., 2001. High speed cnc system design. part i: Jerk limited trajectory generation and quintic spline interpolation 41, 1323–1345.

Ezair, B., Tassa, T., Shiller, Z., 2014. Planning high order trajectories with general initial and final conditions and asymmetric bounds. The International Journal of Robotics Research 33, 898–916.

Jeon, J.W., Ha, Y.Y., 2000. A generalized approach for the acceleration and deceleration of industrial robots and cnc machine tools. IEEE Transactions on Industrial Electronics 74, no 1, 133–139.

Kane, T.R., Ryan, R., Banerjee, A.K., 1987. Dynamics of a cantilever beam attached to a moving base. Journal of Guidance, Control, and Dynamics 10, 139–151.

Kim, D.I., Jeon, J.W., Kim, S., 1994. Software acceleration/deceleration methods for industrial robots and cnc machine tools. Mechatronics 4, 37–53.

Knierim, K.L., Sawodny, O., 2012. Real-time trajectory generation for three-times continuous trajectories, in: 2012 7th IEEE Conference on Industrial Electronics and Applications (ICIEA), pp. 1462–1467.

Kozak, K., Singhose, W., Ebert-Uphoff, I., 2006. Performance measures for input shaping and command generation. Journal of Dynamic Systems Measurement and Control 128, 731–736.

Kroger, T., Tomiczek, A., Wahl, F.M., 2006. Towards on-line trajectory computation, in: 2006 IEEE/RSJ International Conference on Intelligent Robots and Systems, pp. 736–741.

Kroger, T., Wahl, F.M., 2010. Online trajectory generation: Basic concepts for instantaneous reactions to unforeseen events. IEEE Transactions on Robotics 26, 94–111.

Lambrechts, P., Boerlage, M., Steinbuch, M., 2005. Trajectory planning and feedforward design for electromechanical motion systems. Control Engineering Practice 13, 145–157.

Luo, Z.H., Kitamura, N., Guo, B.Z., 1995. Shear force feedback control of flexible robot arms. IEEE Transactions on Robotics and Automation 11, 760–765.

Nguyen, K.D., Ng, T.C., Chen, I.M., 2008. On algorithms for planning s-curve motion profiles. International Journal of Advanced Robotic Systems 5, 11.

Nozawa, R., Kawamura, H., Sasaki, T., 1985. Acceleration/decelaration circuit.

Sencer, B., Ishizaki, K., Shamoto, E., 2015. High speed cornering strategy with confined contour error and vibration suppression for cnc machine tools. CIRP Annals 64, 369 – 372.

Singer, N., Singhose, W., Seering, W., 1999. Comparison of filtering methods for reducing residual vibration. European Journal of Control 5, 208–218.

Singer, N.C., Seering, W.P., 1990. Preshaping command inputs to reduce system vibration. ASME Journal of Dynamic Systems, Measurement, and Control 112, 76–82.

Singhose, W., Singer, N., Seering, W., 1995. Comparison of command shaping methods for reducing residual vibration, in: Third European Control Conf, pp. 1126–1131.

Tajima, S., Sencer, B., Shamoto, E., 2018. Accurate interpolation of machining tool-paths based on fir filtering. Precision Engineering 52, 332 – 344.

Zanasi, R., Bianco, C.G.L., Tonielli, A., 2000. Nonlinear filter for the generation of smooth trajectories. Automatica 36, 439–448.

Zanasi, R., Morselli, R., 2003. Discrete minimum time tracking problem for a chain of three integrators with bounded input. Automatica 39 (9), 1643–1649.

Zheng, C., Su, Y., Muller, P., 2009. Simple online smooth trajectory generations for industrial systems. Mechatronics 19, 571–576.